European Journal of Mechanics B/Fluids 49 (2015) 264–271

Contents lists available at ScienceDirect

European Journal of Mechanics B/Fluids

journal homepage: www.elsevier.com/locate/ejmflu

A measure of axisymmetry for vortex rings

Ahmad Falahatpisheh [a,b], Arash Kheradvar [c,*]

[a] Department of Mechanical and Aerospace Engineering, University of California, Irvine, CA, 92967, USA

[b] Department of Biomedical Engineering, University of California, Irvine, CA, 92967, USA

[c] Edwards Lifesciences Center for Advanced Cardiovascular Technology, The Henry Samueli School of Engineering, University of California, Irvine, CA 92697, USA

ARTICLE INFO

Article history:
Received 26 March 2014
Received in revised form
27 August 2014
Accepted 29 September 2014
Available online 22 October 2014

Keywords:
Axisymmetry index
Vortex ring
Non-axisymmetry
Vortex ring impulse

ABSTRACT

There are many conditions in which a vortex ring deviates from axisymmetry. The shape of a three dimensional vortex ring represents the axisymmetry of propulsion, which has applications in animal locomotion (e.g., the free-swimming of a jellyfish), rocket and marine propulsion devices as well as blood flow through the heart valves. No fluid dynamics' measure is yet defined to quantify the axisymmetry of a three dimensional vortex ring with a single value. The non-axisymmetry exists, for instance, in the vortex ring formed downstream of the mitral valve of healthy hearts, and helps efficient blood momentum transfer from the left atrium toward the aorta. Here, we introduce an index that measures the deviation of a vortex ring from axisymmetry. This index examines the spectrum of the impulse of a naturally-formed vortex ring and expresses the deviation from axisymmetry in terms of the vortex's impulse. We show that the axisymmetry index is related to the second moment of the vorticity distribution of the ring, i.e., as the second moment of vorticity on one side increases compared to the other side, the axisymmetry index decreases accordingly.

1. Introduction

Vortex rings exist in nature wherever "propulsive systems" or "transient jet flows" are present; from flow through the mitral valve to the vortex that pushes a jelly fish forward. Various characteristics related to vortex rings' formation, structure and dynamics have been extensively studied in the past, many of which are well reviewed by Shariff and Leonard [1]. The shape of the vortex ring indicates the degree of axisymmetry of the flow. No fluid dynamics measure currently exists to quantify the axisymmetry of a vortex ring with a single value. Here, we develop an index that quantifies the axisymmetry of vortex rings. This index not only allows differentiating between non-axisymmetric rings but also quantifies their difference, which is important in designing propulsive systems and for diagnostic purposes (e.g., cardiac flows).

There are many conditions in which vortices are non-axisymmetric as have been numerically and experimentally shown. One example is the non-axisymmetric vortex that forms inside a healthy left ventricle of the heart. Non-axisymmetry can be induced either because of an external strain field [2] or due to a nonlinear perturbation of an axisymmetric vortex [3]. The metamorphosis of non-axisymmetric vortices into axisymmetric structures and vice versa has been frequently reported. It has been suggested that non-axisymmetry relaxes to an axisymmetric state for a class of elliptic vortices through the 'axisymmetrization' process [4]. Along the same line, it has been shown that the axisymmetrization process is due to the shear-diffusion averaging mechanism [5,6]. Alternatively, for sufficiently large Reynolds numbers, axisymmetric vortices can evolve into an asymmetric or non-axisymmetric state during a process called 'asymmetrization'. Axisymmetric vortex rings formed along with a starting jet out of a circular nozzle are observed to ultimately become asymmetric. Feng et al. numerically simulated the azimuthal instability for the ring and showed that the ring remains axisymmetric during early formation, but later on undergoes a wavy azimuthal instability [7]. Asymmetrization has been shown to be an indicator of performance and control of aircraft and other flight vehicles capable of extreme maneuvers [8].

For two-dimensional turbulence, the axisymmetrization process results in the circular shape of the vortex [9]. The tendency of isolated and initially non-axisymmetric vortices in becoming axisymmetric by purely inviscid mechanisms has been demonstrated by Dritschel [10]. Dritschel also showed that vortices with sufficiently steep edge gradients can indefinitely remain non-axisymmetric, and further defined the limits for the tendency to axisymmetrization [10]. In 3D flows, O'Farrell and Dabiri [11] studied the variation of vortex formation time on non-axisymmetric

* Correspondence to: 2410 Engineering Hall, University of California, Irvine, CA, 92697, USA. Tel.: +1 949 824 6538.
E-mail address: arashkh@uci.edu (A. Kheradvar).

http://dx.doi.org/10.1016/j.euromechflu.2014.09.003
0997-7546/

vortex rings, formed from different elliptical nozzles [12]. Furthermore, Couch and Krueger [13] experimentally investigated the interaction of vortex rings with oblique surfaces in three dimensions. They studied the symmetry of the flow based on moments of kinetic energy and vorticity around their centroids. In their study, symmetry was defined using three moments of kinetic energy and vorticity. In that study, the symmetry of the flow was investigated with respect to planes and axisymmetry of the vortex ring with respect to its axis was not addressed.

In this study, we introduce an index to quantify the degree of non-axial-symmetry for vortex rings generated behind a nozzle or in other propulsive systems. We systematically examine the performance of the index for a range of vortex structures in analytical vortex rings and in realistic computational fluid dynamics (CFD) cases.

2. Methods and results

In this section, we describe an index to assess the axisymmetry of 3D vortex rings. Here, by a vortex ring, we refer to any closed vorticity structure (one complete ring) that can be either axisymmetric or non-axisymmetric. In other words, a vorticity patch in an otherwise "almost" irrotational flow field, where "almost" stands for the possible presence of others "isolated" structures that do not directly interact with each other (in terms of distances comparable with the viscous length-scale).

According to Batchelor [14], the impulse for a general vortex ring, $\mathbf{I}_\mathrm{v}$, is

$$\mathbf{I}_\mathrm{v} = \frac{\rho}{2}\int \boldsymbol{x}\times\boldsymbol{\omega}\mathrm{d}V, \tag{1}$$

where $\boldsymbol{x}$ is the position vector, $\boldsymbol{\omega}$ is the vorticity vector, and V is the volume of the fluid where the ring is located. For an axisymmetric vortex ring, Eq. (1) simplifies to $\mathbf{I}_\mathrm{a}$ [1], as follows

$$\mathbf{I}_\mathrm{a} = I_\mathrm{a}\hat{\mathbf{x}} = \pi\rho\hat{\mathbf{x}}\int \omega_\theta(x,\sigma)\,\sigma^2\mathrm{d}x\mathrm{d}\sigma, \tag{2}$$

where $\hat{\mathbf{x}}$ is the axis of the ring; ρ is the density of the fluid; ω_θ is the vorticity distribution in any azimuthal plane θ; and x and σ are the axial and radial coordinates, respectively.

In contrast to an axisymmetric vortex ring, the circulation, Γ, of a non-axisymmetric ring is not inevitably constant, as some vortex lines can escape from the ring on one side and attach either to the wake on the other side or to the upstream boundary layer [15]. Because of this, we computed the equivalent axisymmetric impulse by examining the spectrum of axisymmetric impulses, $\mathbf{I}_{\mathrm{a}\theta}$, at multiple θ-planes. A θ-plane is a plane that sections the vortex ring and passes through the axis of the ring while making an angle θ with the reference plane.

The radial vorticity centroid [1] for each θ-plane is defined as

$$R_\theta = \frac{\int_{A_\theta}\sigma\omega_\theta(x,\sigma)\,\mathrm{d}x\mathrm{d}\sigma}{\int_{A_\theta}\omega_\theta(x,\sigma)\,\mathrm{d}x\mathrm{d}\sigma}. \tag{3}$$

The axisymmetric impulse for each θ-plane is

$$\mathbf{I}_{\mathrm{a}\theta} = I_{\mathrm{a}\theta}\hat{\mathbf{x}} = \pi\rho\hat{\mathbf{x}}\int_{A_\theta}\omega_\theta(x,\sigma)\,\sigma^2\mathrm{d}A_\theta, \tag{4}$$

where A_θ is the area of the θ-plane whose extent is from the axis of the ring to either the boundary of the domain or infinity, and makes an angle θ with respect to the axis. $\bar{I}_\mathrm{a}$ is the average of all the impulses of the θ-planes and is called the impulse threshold, i.e., the average of $\mathbf{I}_{\mathrm{a}\theta}$s

$$\bar{I}_\mathrm{a} = \frac{1}{2\pi}\int_0^{2\pi}\|\mathbf{I}_{\mathrm{a}\theta}\|\mathrm{d}\theta = \frac{1}{N}\sum_{i=1}^{N}\|\mathbf{I}_{\mathrm{a}\theta}\|, \tag{5}$$

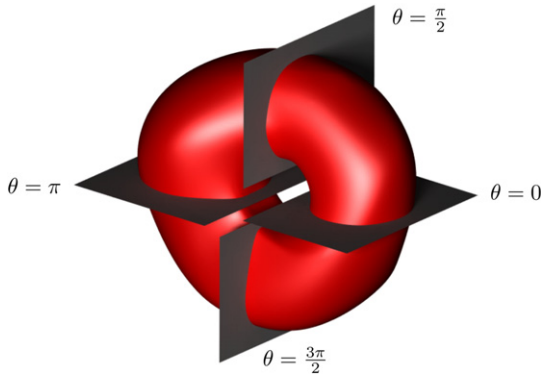

Fig. 1. An example of a non-axisymmetric vortex ring. Planes shown in the figure represent the planes where the axisymmetric impulse, $\mathbf{I}_{\mathrm{a}\theta}$ is calculated. The area $\mathbf{A}_\theta$ is the area of the θ-planes (from $\theta = 0,\ldots,2\pi$) whose extent is from the axis of the ring to infinity. In the figure, only a portion of four θ-planes are shown, as examples.

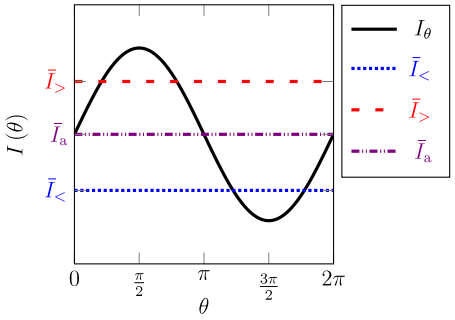

Fig. 2. An example of the spectrum of the vortex ring impulse at different θ-planes. $\bar{I}_\mathrm{a}, \bar{I}_<, \bar{I}_>$ are three representatives of any impulse spectrum that are used to define the axisymmetry index, $\xi = \frac{\bar{I}_<}{\bar{I}_>}$.

where N is the number of θ-planes. In this study, using 72 θ-planes, $\theta = 0, \frac{5\pi}{360}, \ldots, \frac{715\pi}{360}$ with respect to the axis of the ring and with a resolution of 100×100, provided the convergency of the results, as schematically shown in Fig. 1. Depending on the complexity of the vortex ring, increasing the number of θ-planes might yield more accurate values for the equivalent axisymmetric impulses and therefore, must be checked for convergency of the results. It should be noted that for calculation of $\mathbf{I}_{\mathrm{a}\theta}$, each θ-plane is assumed to be an axisymmetric plane in its own (x,σ) coordinate system. We describe the axisymmetry index, ξ, to be a non-dimensional impulse

$$\xi = \frac{\bar{I}_<}{\bar{I}_>} \tag{6}$$

where $\bar{I}_<$ is the average of all the impulses that are less than the impulse threshold, i.e., $I_\theta < \bar{I}_\mathrm{a}$. Similarly, $\bar{I}_>$ is the average of all the impulses that are greater than the impulse threshold, i.e., $I_\theta > \bar{I}_\mathrm{a}$. This concept is further clarified in Fig. 2.

The circulation in each θ-plane is found by

$$\Gamma_\theta = \int_{A_\theta}\boldsymbol{\omega}_\theta\cdot\mathrm{d}\mathbf{A}_\theta. \tag{7}$$

The mean circulation and mean radial vorticity centroid are defined as

$$\bar{\Gamma}_\mathrm{a} = \frac{1}{N}\sum_{i=1}^{N}\Gamma_\theta, \qquad \bar{R}_\mathrm{a} = \frac{1}{N}\sum_{i=1}^{N}R_\theta. \tag{8}$$

For an axisymmetric vortex ring, ξ is equal to unity as there is no difference between $\bar{I}_<$ and $\bar{I}_>$. The less the difference, the more

axisymmetric the vortex ring is. Once the vortex ring deviates from axisymmetry, ξ deviates from unity. This deviation in the impulse ratio is described in Eq. (6) and can be due to the eccentricity of the vortex ring centroid, which is linked to a non-axisymmetric distribution of circulation, Γ_θ, radial vorticity centroid, R_θ, and impulse, I_θ, among all the θ-planes. In other words, the more uniform the I_θ-spectrum is, the more axisymmetric the vortex ring is. Consequently, an axisymmetric ring is only represented by one impulse value: $\bar{I}_a$ while a non-axisymmetric vortex ring possesses three distinct representatives: $\bar{I}_a$, $\bar{I}_<$, and $\bar{I}_>$.

The axisymmetry of the 3D naturally-formed vortex ring is measured with respect to $(\bar{x}_\omega, \bar{y}_\omega, \bar{z}_\omega)$, which is the center of the 3D vorticity distribution, $\boldsymbol{\omega}(x, y, z)$,

$$(\bar{x}_\omega, \bar{y}_\omega, \bar{z}_\omega) = \left(\frac{\sum_V x\|\boldsymbol{\omega}\|\Delta V}{\sum_V \|\boldsymbol{\omega}\|\Delta V}, \frac{\sum_V y\|\boldsymbol{\omega}\|\Delta V}{\sum_V \|\boldsymbol{\omega}\|\Delta V}, \frac{\sum_V z\|\boldsymbol{\omega}\|\Delta V}{\sum_V \|\boldsymbol{\omega}\|\Delta V} \right), \quad (9)$$

where x, y, and z are the Cartesian coordinates; $\|\boldsymbol{\omega}\|$ is the magnitude of the vorticity; and ΔV is the finite cell volume. The centroid and the axis of the ring are used in defining the θ-planes as well as in the calculation of ξ. Alternatively, the vortex ring centroid can be found by the methods described by Chong et al. [16], Braun et al. [17], or Ouellette and Gollub [18]. For the cases where no information is available about the axis of the propulsion or transient jet, one may use Principal Component Analysis to obtain the axes of the ring.

In the following sections, we describe a systematic validation for the axisymmetry index, ξ, in analytically and numerically obtained vortex rings. First, we validate ξ for a Gaussian vortex ring in an axisymmetric plane. Since a non-axisymmetric vortex ring is a 3D flow structure, the performance of ξ in three dimensions is examined. To test this, we utilize Hill's spherical vortex [19] as a 3D benchmark for ξ. Additionally, several non-axisymmetric vortex rings are generated by asymmetrically revolving the Gaussian vorticity distribution around the axis. Finally, we examine the axisymmetry of a vortex that is numerically formed from an oval-shaped nozzle.

2.1. Gaussian vortex ring

First, we examine the axisymmetry index, ξ, for a Gaussian vortex ring whose vorticity field is defined by [20] as follows

$$\omega_\theta(x, \sigma) = \frac{\Gamma}{\pi {R_c}^2} \exp\left[-\frac{(x - x_0)^2 + (\sigma - R_0)^2}{{R_c}^2} \right], \quad (10)$$

where σ is the distance from the axis, Γ is the circulation, R_c is the core radius, and (x_0, R_0) are the coordinates of the Gaussian vortex ring location.

A Gaussian vortex ring was generated using Eq. (10) in the $x\sigma$-plane, as shown in Fig. 3(a). The ring was located at $R_0 = 5.0$ and $x_0 = 5.0$, with $R_c = 0.5$ and $\Gamma = 1.0$ at the domain of $x \in [0, 10.0]$ and $\sigma \in [0, 10.0]$. The vorticity distribution was revolved around the axis in a grid of $100 \times 100 \times 100$ to compute the axisymmetry index, as shown in Fig. 3(b). In this case, ξ was found to be 0.9965.

2.2. Hill's spherical vortex (HSV)

HSV is a convenient example for the purpose of validation [19]. This vortex is an extreme member of the Norbury family vortex rings [21], which is used as a model in applications such as the motion of bubbles and droplets at high Reynolds number. The vorticity inside the HSV varies linearly with the distance from the axis of symmetry, while the vorticity outside the HSV is zero. In a HSV, the external flow is irrotational around a sphere whereas the internal flow possesses an axisymmetric vorticity distribution.

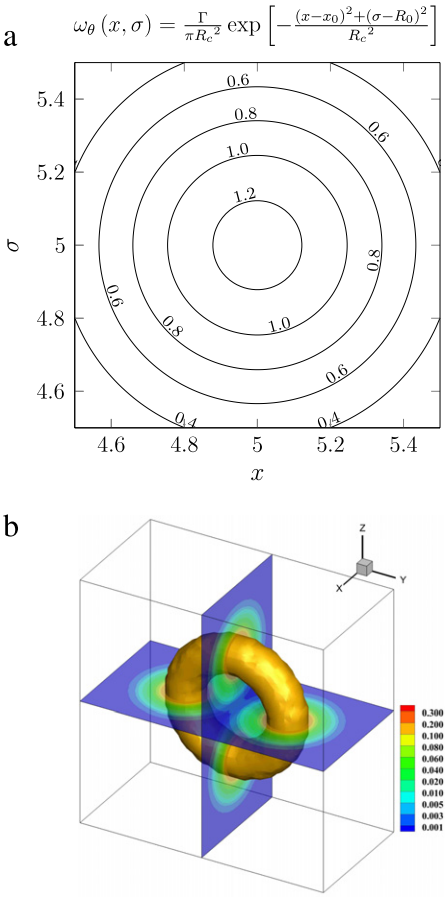

Fig. 3. A Gaussian vortex ring. (a) Gaussian vorticity distribution. The ring was located at $R_0 = 5.0$ and $x_0 = 5.0$, with $R_c = 0.5$ and $\Gamma = 1.0$. (b) The isosurface of vorticity magnitude $\|\boldsymbol{\omega}\| = 0.14\ s^{-1}$ is used to illustrate the ring. Contours of vorticity magnitude are also shown.

The HSV is described by two velocity fields. The internal field, $\mathbf{u}^i$, is defined for points inside the unit sphere $r = \sqrt{x^2 + y^2 + z^2} \leq 1$ and the external velocity field, $\mathbf{u}^o$, is when the points lie outside the sphere ($r \geq 1$)

$$\mathbf{u}^i(x, y, z) = \begin{pmatrix} x^2 + 1 - 2r^2 \\ xy \\ xz \end{pmatrix}, \quad (11a)$$

$$\mathbf{u}^o(x, y, z) = \begin{pmatrix} z^2 r^{-5} - \frac{1}{3} r^{-3} - \frac{2}{3} \\ xyr^{-5} \\ xzr^{-5} \end{pmatrix}. \quad (11b)$$

This results in a linear vorticity field distribution inside the sphere

$$\omega_x = 0, \quad (12a)$$

$$\omega_y = -5z, \quad (12b)$$

$$\omega_z = 5y, \quad (12c)$$

while the vorticity is zero everywhere outside ($r \geq 1$). Eqs. (11a) and (11b) create a HSV whose axis is along the x-axis.

A HSV, with the centroid at the origin in a domain of $1.5 \times 1.5 \times 1.5$ was studied. The HSV vorticity distribution was populated in $100 \times 100 \times 100$ grid. For HSV, the axisymmetry index was found to be 0.9917.

2.3. Parametric generation of non-axisymmetric vortex rings

In this section, we describe how we artificially generated non-axisymmetric vortex rings. In fact, non-axisymmetry can be found

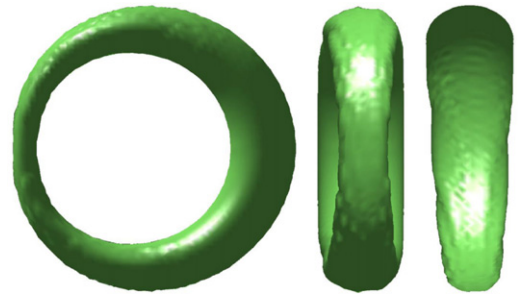

(a) $\rho = 3.8$.

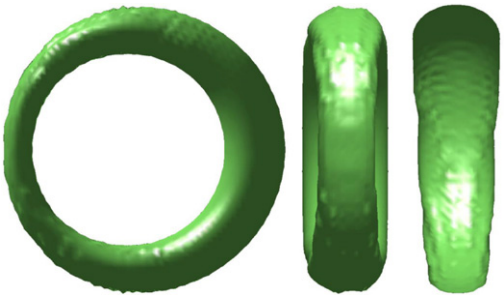

(b) $\rho = 4.9$.

(c) $\rho = 105$.

Fig. 4. Different views of three vortex rings generated by different revolving factors shown by isosurfaces of vorticity magnitude $\|\boldsymbol{\omega}\| = 0.05\ \mathrm{s}^{-1}$. The ring was located at $R_0 = 5.0$ and $x_0 = 5.0$, with $R_c = 0.5$ and $\Gamma = 1.0$ at the domain of $x \in [0, 10.0]$ and $\sigma \in [0, 10.0]$ in the $x\sigma$-plane. The vorticity distribution was then revolved around the x-axis with different parameters. The domain has a resolution of $100 \times 100 \times 100$. (a) shows a non-axisymmetric vortex ring with $\rho = 3.8$ with $\xi = 0.3136$. (b) illustrates a non-axisymmetric vortex ring generated by $\rho = 4.9$ with $\xi = 0.3873$. (c) depicts a vortex ring created by $\rho = 105$ with $\xi = 0.9781$. Views in each row and from left to right are the yz-plane, xz-plane, xy-plane, respectively.

in a wide variety of forms and the ones created in this section are only examples to test the performance of the index. To produce a non-axisymmetric vortex ring in three dimensions, (x, σ) was parametrically transformed to (x, y, z) by

$$x = x, \tag{13a}$$

$$y = \sigma \cos(\alpha), \tag{13b}$$

$$z = \sigma \sin(\alpha), \tag{13c}$$

where α varies from 0 to 2π. In fact, (x, σ) coordinates were revolved around the x-axis to generate a 3D field. To introduce non-axisymmetry in the vorticity distribution, we utilized the following revolving relations for the coordinates

$$x = x\,[\rho + \cos(\alpha)]^n, \tag{14a}$$

$$y = \sigma \cos(\alpha)\,[\rho + \cos(\alpha)]^m, \tag{14b}$$

$$z = \sigma \sin(\alpha)\,[\rho + \cos(\alpha)]^m, \tag{14c}$$

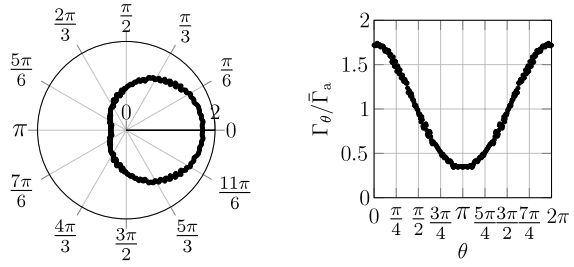

(a) Circulation.

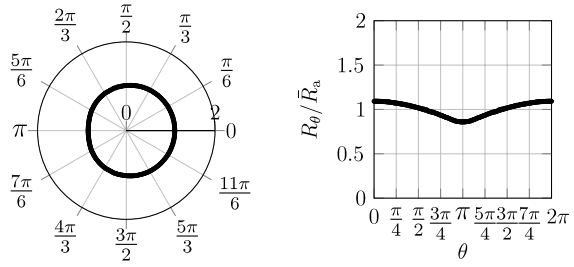

(b) Radial vorticity centroid.

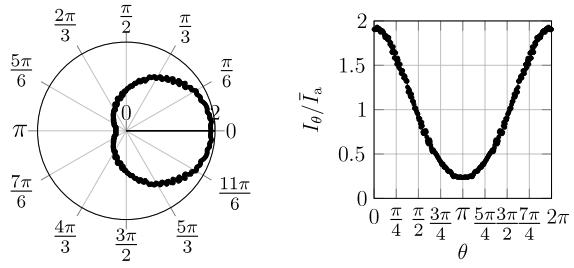

(c) Impulse.

Fig. 5. Spectrum of circulation, Γ_θ, radial vorticity centroid, R_θ, and impulse, I_θ, in 72 θ-planes for the non-axisymmetric vortex ring parametrically created by $\rho = 3.8$. The left figures represent a polar distribution while the ones on right are a linear distribution versus the angle each θ-plane makes with respect to the xy-plane. The axisymmetry index for this vortex ring is $\xi = 0.3136$.

where ρ is the revolving factor and varied from 2.3 to 105, $n = 1$, and $m = 2$. $\rho = 2.3$ creates the most non-axisymmetric ring in the set and $\rho = 105$ creates an axisymmetric one. Eq. (14) introduces non-axisymmetry both axially and radially. In addition, in the process of revolving, the vorticity at point (x, σ) is mapped to point (x, y, z), i.e., $\omega_\theta(x, \sigma) \mapsto \boldsymbol{\omega}(x, y, z)$, according to

$$\omega_x = 0, \tag{15a}$$

$$\omega_y = -\omega_\theta \sin(\alpha), \tag{15b}$$

$$\omega_z = \omega_\theta \cos(\alpha). \tag{15c}$$

By using Eqs. (10), (14), and (15) along with different values for the revolving factor, 50 Gaussian three dimensional vortex rings were created with different degrees of axisymmetry. For each case, the ring was located at $R_0 = 5.0$ and $x_0 = 5.0$, with $R_c = 0.5$ and $\Gamma = 1.0$ at the domain of $x \in [0, 10.0]$ and $\sigma \in [0, 10.0]$. The resolution of the grid was $100 \times 100 \times 100$. Three of the generated vortex rings ($\rho = 3.8$, $\rho = 4.9$, and $\rho = 105$) are illustrated in Fig. 4, as examples. Figs. 5 and 6 show the variation of circulation, radial vorticity centroid, and impulse among θ-planes when $\rho = 3.8$ and $\rho = 105$. By varying the revolving factor, ρ, from 2.3 to 105, the broadness of the circulation spectrum in the θ-planes of each ring became narrower. In other words, the ratio of the maximum to the minimum circulation, $\Gamma_{\max}/\Gamma_{\min}$, for each vortex ring decreased from 15.9905 to 1.0705 and approached unity. Different revolving factors resulted in variation of the axisymmetry index from 0.2035 to 0.9781. Fig. 7 shows the variation

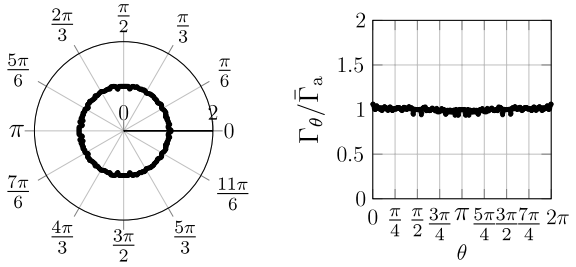

(a) Circulation.

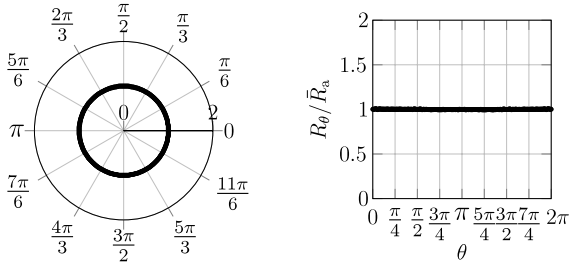

(b) Radial vorticity centroid.

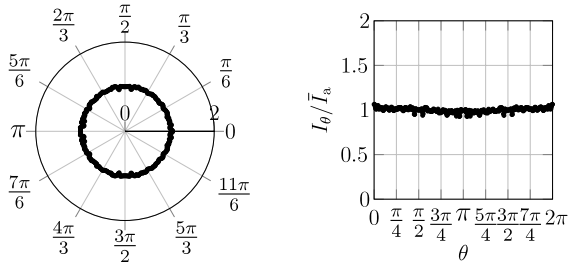

(c) Impulse.

Fig. 6. Spectrum of the circulation, Γ_θ, radial vorticity centroid, R_θ, and impulse, I_θ, in 72 θ-planes for the non-axisymmetric vortex ring created parametrically by $\rho = 105$. The left figures represent a polar distribution while the ones on right are a linear distribution versus the angle each θ-plane makes with respect to the xy-plane. The axisymmetry index for this vortex ring is $\xi = 0.9781$.

of axisymmetry index, ξ, versus the broadness of the spectrum of three features of each vortex ring: circulation, radial vorticity centroid, and impulse. As the ratio of the circulation approached unity, the axisymmetry index asymptotically approached unity as well (Fig. 7). Alternatively when the $\Gamma_{max}/\Gamma_{min}$ increased, the axisymmetry index nonlinearly deviated from unity. Similar observations were found for the radial vorticity centroid and impulse of the ring. By varying from $\rho = 2.3$ to $\rho = 105$, the ratio of the maximum to minimum of the radial vorticity centroid decreased from 1.4706 to 1.0045 (Fig. 7(b)). Also, the ratio of maximum to minimum of impulse of θ-planes reduced from 34.7087 to 1.072 (Fig. 7(c)).

2.4. Non-axisymmetric vortex ring downstream of an oval-shaped nozzle

Here we examined the axisymmetry index in a realistic vortex ring formed downstream of an oval-shaped nozzle. The ring was numerically created in a piston-cylinder mechanism, as shown in Fig. 8. The geometry of the domain was designed such that the axis of the cylinder was the x-axis. ANSYS Fluent 13.0 (Ansys Inc., Cecil Township, PA, USA) was used for the simulation. Because of the symmetry of the problem, only half of the domain was modeled. The boundary condition for the inlet of the oval was a constant velocity $U_{max} = 0.04$ m/s. Equivalent diameter of the oval was $D_e = 0.05680$ m. The fluid was water, and the Reynolds number, $Re = \rho U_{max} D_e/\mu$, was 2048. Boundary conditions on the lateral

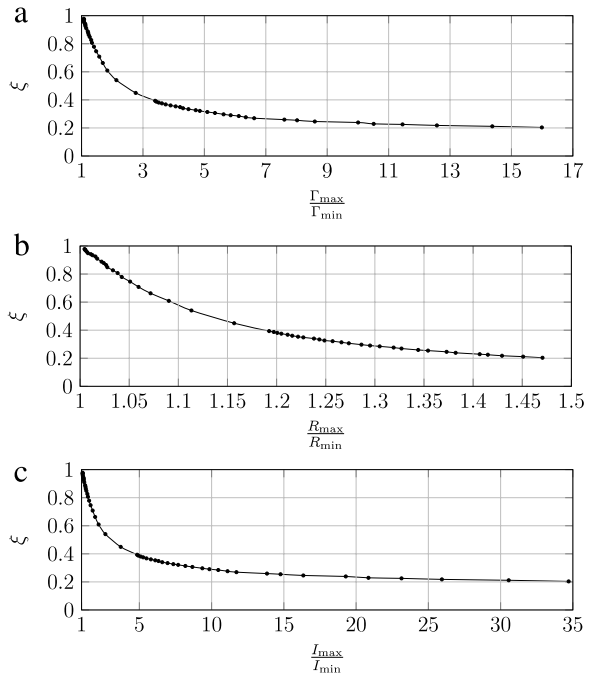

Fig. 7. Axisymmetry index, ξ, versus the ratio of extreme values of circulation, radial vorticity centroid, and impulse. Each graph has 50 data points. (a) shows ξ versus the ratio of the maximum to minimum circulation of the ring, $\Gamma_{max}/\Gamma_{min}$, in θ-planes, (b) illustrates ξ versus the ratio of the maximum to minimum radial vorticity centroid of the ring, R_{max}/R_{min}, in θ-planes, and (c) shows ξ versus the ratio of the maximum to minimum impulse of the ring, I_{max}/I_{min}, in θ-planes. The plateau for ξ occurs when I_{max}/I_{min} is greater than 34, according to the parametric equations (14) and (15), which could not generate more non-axisymmetric rings and asymptotically approached 0.2035 (corresponds to revolving factor $\rho = 2.3$).

and bottom wall of the flow domain as well as the surfaces of the oval cylinder were all no-slip boundary conditions. We assumed that the free surface at the top boundary of the tank does not considerably vary and therefore, considered to be an outflow boundary condition. The simulation continued until $L/D_e = tU_{max}/D_e = 2.51$. Fig. 9(a) shows a formed vortex ring downstream of the nozzle at time 3.56 s ($L/D_e = 2.51$). Fig. 9(b) illustrates the vorticity distribution in two planes. The axisymmetry index for this case was calculated as $\xi = 0.84$. In other words, the formed ring deviated approximately 16% from axisymmetry. The spectrum of non-dimensional circulation, radial vorticity centroid, and impulse are shown in Fig. 10. The evolution of the vortex ring with time is shown in Fig. 11. Axisymmetry of the ring increased, followed by a decrease when $L/D_e < 0.2$. The ring then showed a monotonic increase shortly after its formation.

3. Discussion

Vortex rings occurring in nature have been identified as important flow features. The shape of a vortex ring is proven to be an important feature of blood flow in the heart. Kilner et al. emphasized the significance of the asymmetry of the flow through the heart cavities [22]. The shape of the transmitral vortex ring that develops during the filling phase of the left ventricle has been shown to be a measure of diastolic function [23] as well as being a tool to assess the mitral valve [24].

To date, vortices have been examined from many different perspectives and in diverse applications including aerospace [8], cardiac flows [22,23,25,26], and free-swimming jellyfish [27,28]. However, no study has yet discussed the measurement of the inherited non-axisymmetry of vortex rings with a single value.

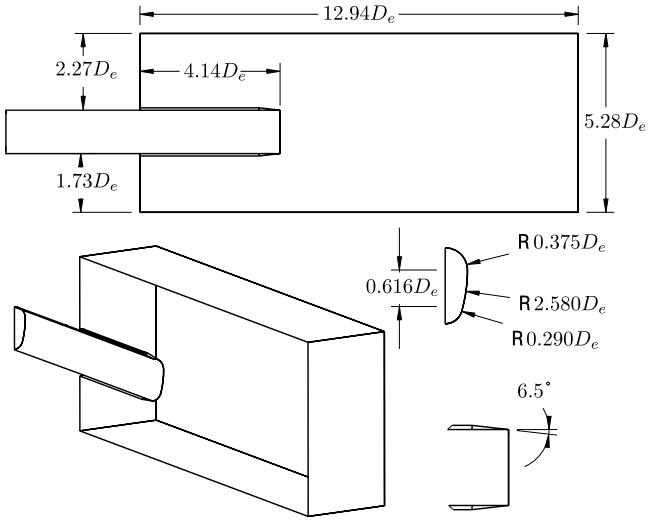

Fig. 8. Domain of the CFD model, dimensions of the oval-shaped nozzle, and the wedge angle at the nozzle. Equivalent diameter of the oval is $D_e = 0.05680$ m.

We studied our developed axisymmetric index, ξ, for several different vortex ring cases. The index was assessed against the variation of the ratio of extreme values in the spectrum of circulation, radial vorticity centroid, and impulse, i.e. $\Gamma_{max}/\Gamma_{min}$, R_{max}/R_{min}, and I_{max}/I_{min}. We found that the ratio of the extremes of circulation, radial vorticity centroid, and impulse are all directly correlated with the deviation of the vortex ring from axisymmetry. As a result, the broader the spectrum of circulation, radial vorticity centroid, and impulse, the less the axisymmetry index is, and hence, the more non-axisymmetric the vortex is. In other words, as the degree of non-uniformity in the distribution of the second moment of vorticity about a vortex ring's axis is increased (i.e., the impulse on one side of the ring is a factor of the impulse of the other side), the value for ξ decreases accordingly. Furthermore, as this non-uniformity tends to vanish (i.e. the ratio of maximum to minimum of Γ, R, and I tends to unity), the change in axisymmetry becomes steep while its variation loses sensitivity at higher degrees of non-uniformity.

According to Couch and Krueger [13], symmetry with respect to planes was investigated by three vorticity moments. However, one needs to combine them in order to measure the axisymmetry with

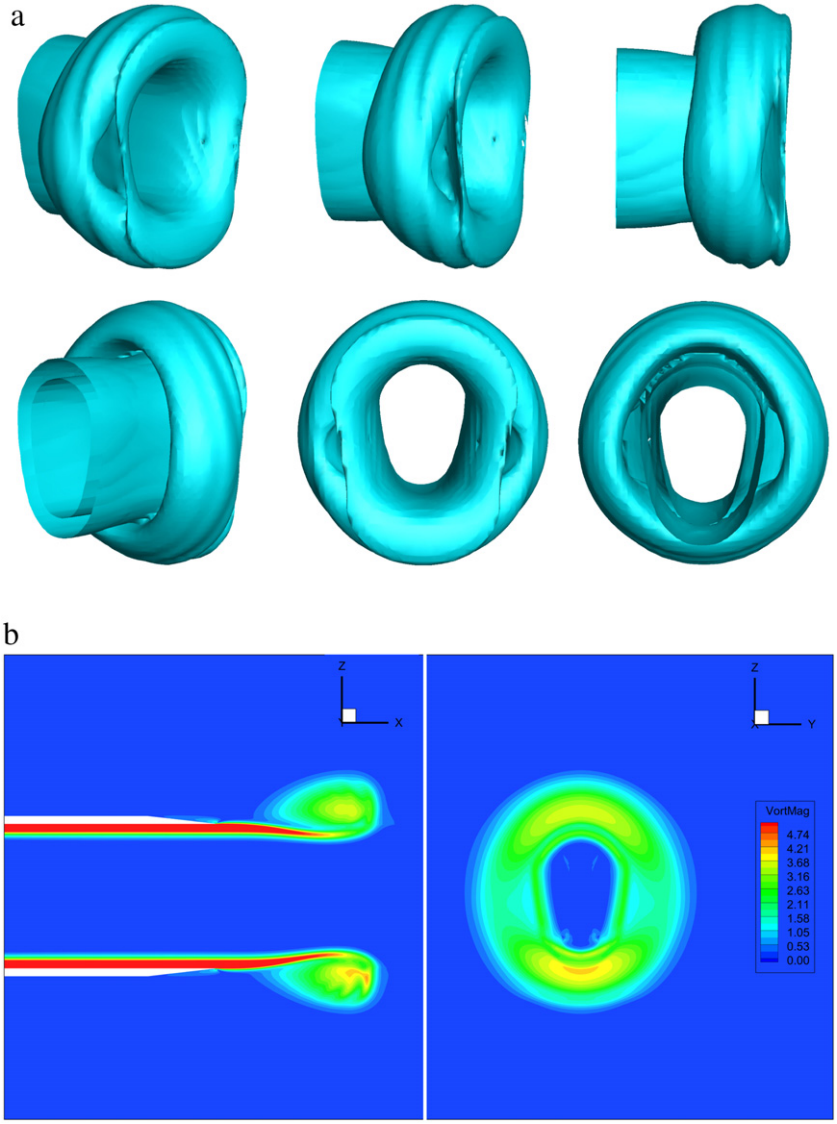

Fig. 9. (a) Isosurfaces of vorticity magnitude, $\|\boldsymbol{\omega}\| = 2.22\ s^{-1}$ for the CFD case at non-dimensional time $L/D_e = 2.51$. Six different views of the same vortex ring are shown for better illustration of the ring's non-axisymmetry ($\xi = 0.84$). (b) The vorticity distribution in two planes.

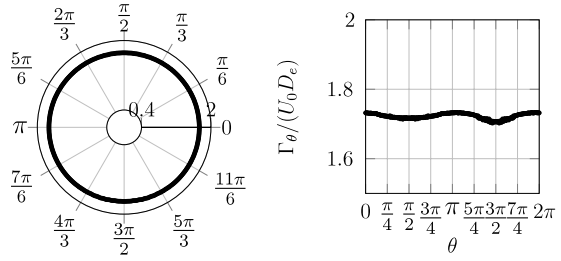

(a) Circulation.

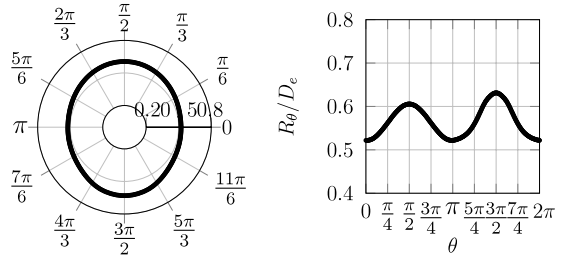

(b) Radial vorticity centroid.

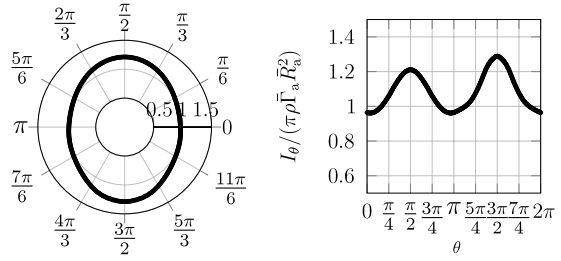

(c) Impulse.

Fig. 10. Spectrum of circulation, Γ_θ, radial vorticity centroid, R_θ, and impulse, I_θ, in 72 θ-planes for the non-axisymmetric vortex ring resulted from CFD. Figures on the left represent a polar distribution while the ones on the right are a linear distribution versus the angle that each θ-plane makes with the xy-plane. The values are non-dimensionalized by inlet velocity, U_0, equivalent diameter of the nozzle, D_e, density of the fluid, ρ, the average of the circulation, $\bar{\Gamma}_a$, and average of the radial vorticity centroid, $\bar{R}_a$. The plotted I_θ is divided by the density of the fluid. ξ was found to be 0.84.

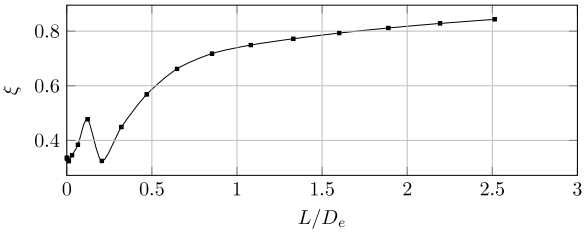

Fig. 11. Axisymmetry versus non-dimensional time L/D_e for the CFD case.

one single value. Here, we defined this combination as

$$\xi' = 1 - \frac{\omega_{12}^2 + \omega_{13}^2 + \omega_{23}^2}{\omega_{11}^2 + \omega_{22}^2 + \omega_{33}^2} \tag{16}$$

where ω_{ij} is the vorticity moments ($i = 1, 2, 3$ and $j = 1, 2, 3$), as defined in [13]. With this definition, this index yields results between 0 and 1 that can be compared with Eq. (6). The comparison is shown in Fig. 12. As can be seen, the sensitivity of $\xi = \frac{\bar{I}_<}{\bar{I}_>}$ to axisymmetry is greater than the metrics developed based on the concept introduced by Couch and Krueger.

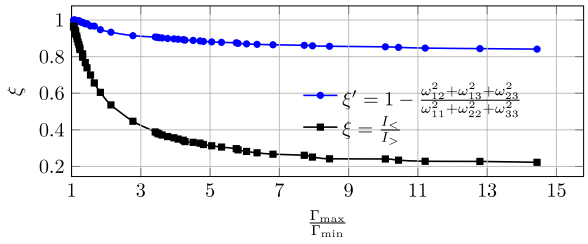

Fig. 12. The comparison between Eq. (16) and $\xi = \frac{\bar{I}_<}{\bar{I}_>}$ for the non-axisymmetric vortex rings family (Eqs. (14) and (15)).

It should be noted that ξ and ξ' are both positive numbers ≤ 1. According to Eq. (6), when $\xi = 0$, it implies that $\bar{I}_<$ should be absolutely zero. This cannot physically exist as $\bar{I}_<$ is the average of the impulses of the spectrum that is less than the threshold defined by Eq. (5). Therefore, $\bar{I}_<$ is a non-zero number. However, if theoretically, $\bar{I}_<$ would be orders of magnitude smaller than $\bar{I}_>$, i.e., $\mathcal{O}(\bar{I}_<) \ll \mathcal{O}(\bar{I}_>)$, then axisymmetry index, ξ, would approach zero. In other words, the vortex ring would possess a very broad spectrum, which would cause a huge difference between $\bar{I}_<$ and $\bar{I}_>$. As a result, ξ is a positive number ≤ 1.

Similar to ξ, ξ' is a positive number ≤ 1. In order for ξ' to become zero, $\omega_{12}^2 + \omega_{13}^2 + \omega_{23}^2$ should be equal to $\omega_{11}^2 + \omega_{22}^2 + \omega_{33}^2$. This implies that the summation of strengths of the off-diagonal vorticity moments is the same as that of the diagonal terms. For propulsive systems as well as the transient jets, $\omega_{12}^2 + \omega_{13}^2 + \omega_{23}^2$ is always less than $\omega_{11}^2 + \omega_{22}^2 + \omega_{33}^2$. This limits ξ' to values larger than zero. In addition, adding an exponent, n, to Eq. (16), i.e., $\xi' = 1 - \left[\left(\omega_{12}^2 + \omega_{13}^2 + \omega_{23}^2\right) / \left(\omega_{11}^2 + \omega_{22}^2 + \omega_{33}^2\right)\right]^n$, allows ξ' to be more sensitive to the variation of the vorticity moments. However, even improving the sensitivity of ξ' would not provide the capability to correctly evaluate the symmetry around an axis. This is due to the inherent dependency of ξ' on vorticity moments with respect to Cartesian coordinate planes. Because of this definition, there can be non-axisymmetric vortices for which $\xi' = 1$, which therefore limits the application of ξ' to measuring symmetry rather than axisymmetry.

4. Conclusions

A quantitative measure of axisymmetry is developed based on the comparison of a naturally-formed vortex ring with equivalent axisymmetric rings, as discussed in the methods section. We tested the performance of the index in the analytical cases of Gaussian vortex rings and Hill's spherical vortex. For these cases, the axisymmetry index, ξ was found to be in close agreement with the axisymmetric nature of the rings (i.e., $\xi = 1.0$). Furthermore, a series of independent non-axisymmetric vortex rings were parametrically generated in three dimensions and their ξ were studied versus the ratio of the maximum to minimum of circulation, radial vorticity centroid, and impulse. The axisymmetry index was found to be correlated to the second moment of vorticity about the vortex ring's axis. As the second moment of vorticity on one side increases compared to the other side, the axisymmetry index decreases accordingly. The index was also examined in the evolution of the formed vortex ring in a realistic CFD case in which the nozzle was oval-shaped. The ring showed a monotonic increase in axisymmetry shortly after its formation.

Acknowledgments

This work has been supported by a postdoctoral fellowship (14POST20530013) from the American Heart Association to Dr. Falahatpisheh and a Transatlantic Career Award from the Fondation Leducq to Dr. Kheradvar.

References

[1] K. Shariff, A. Leonard, Vortex rings, Annu. Rev. Fluid Mech. 24 (1) (1992) 235–279.
[2] J. Jimenez, H. Moffatt, C. Vasco, The structure of the vortices in freely decaying two-dimensional turbulence, J. Fluid Mech. 313 (1996) 209–222.
[3] L.F. Rossi, J.F. Lingevitch, A.J. Bernoff, Quasi-steady monopole and tripole attractors for relaxing vortices, Phys. Fluids 9 (1997) 2329.
[4] M. Melander, J. McWilliams, N. Zabusky, Axisymmetrization and vorticity-gradient intensification of an isolated two-dimensional vortex through filamentation, J. Fluid Mech. 178 (1) (1987) 137–159.
[5] A.J. Bernoff, J.F. Lingevitch, Rapid relaxation of an axisymmetric vortex, Phys. Fluids 6 (11) (1994) 3717–3723. (1994-present).
[6] T. Lundgren, Strained spiral vortex model for turbulent fine structure, Phys. Fluids 25 (1982) 2193.
[7] H. Feng, L. Kaganovskiy, R. Krasny, Azimuthal instability of a vortex ring computed by a vortex sheet panel method, Fluid Dynam. Res. 41 (5) (2009) 051405.
[8] J. Cai, S. Luo, F. Liu, Stability of symmetric and asymmetric vortex pairs over slender conical wings and bodies, Phys. Fluids 16 (2) (2004) 424–432.
[9] J.C. McWilliams, The emergence of isolated coherent vortices in turbulent flow, J. Fluid Mech. 146 (1) (1984) 21–43.
[10] D.G. Dritschel, On the persistence of non-axisymmetric vortices in inviscid two-dimensional flows, J. Fluid Mech. 371 (1) (1998) 141–155.
[11] C. O'Farrell, J.O. Dabiri, Pinch-off of non-axisymmetric vortex rings, J. Fluid Mech. 740 (2014) 61–96.
[12] M. Gharib, E. Rambod, A. Kheradvar, D.J. Sahn, J.O. Dabiri, Optimal vortex formation as an index of cardiac health, Proc. Natl. Acad. Sci. 103 (16) (2006) 6305–6308.
[13] L.D. Couch, P.S. Krueger, Experimental investigation of vortex rings impinging on inclined surfaces, Exp. Fluids 51 (4) (2011) 1123–1138.
[14] G.K. Batchelor, An Introduction to Fluid Dynamics, Cambridge University Press, 1973.
[15] F. Domenichini, Three-dimensional impulsive vortex formation from slender orifices, J. Fluid Mech. 666 (2011) 506–520.
[16] M. Chong, A. Perry, B. Cantwell, A general classification of three-dimensional flow fields, Phys. Fluids A 2 (5) (1990) 765–777. 1989-1993.
[17] W. Braun, F. De Lillo, B. Eckhardt, Geometry of particle paths in turbulent flows, J. Turbul. 7 (2006) N62. http://dx.doi.org/10.1080/14685240600860923.
[18] N.T. Ouellette, J.P. Gollub, Curvature fields, topology, and the dynamics of spatiotemporal chaos, Phys. Rev. Lett. 99 (19) (2007) 194502.
[19] M.J.M. Hill, On a spherical vortex, Proc. R. Soc. Lond. 55 (331–335) (1894) 219–224.
[20] Y. Hattori, S.G.L. Smith, Axisymmetric acoustic scattering by vortices, J. Fluid Mech. 473 (2002) 275–294.
[21] J. Norbury, A family of steady vortex rings, J. Fluid Mech. 57 (3) (1973) 417–431.
[22] P.J. Kilner, G.-Z. Yang, A.J. Wilkes, R.H. Mohiaddin, D.N. Firmin, M.H. Yacoub, Asymmetric redirection of flow through the heart, Nature 404 (6779) (2000) 759–761.
[23] A. Kheradvar, R. Assadi, A. Falahatpisheh, P.P. Sengupta, Assessment of transmitral vortex formation in patients with diastolic dysfunction, J. Amer. Soc. Echocardiogr. 25 (2) (2012) 220–227.
[24] A. Kheradvar, A. Falahatpisheh, The effects of dynamic saddle annulus and leaflet length on transmitral flow pattern and leaflet stress of a bileaflet bioprosthetic mitral valve, J. Heart Valve Disease 21 (2) (2012) 225.
[25] G. Pedrizzetti, F. Domenichini, Nature optimizes the swirling flow in the human left ventricle, Phys. Rev. Lett. 95 (10) (2005) 108101.
[26] T. Schenkel, M. Malve, M. Reik, M. Markl, B. Jung, H. Oertel, MRI-based CFD analysis of flow in a human left ventricle: methodology and application to a healthy heart, Ann. Biomed. Eng. 37 (3) (2009) 503–515.
[27] J.O. Dabiri, S.P. Colin, J.H. Costello, Fast-swimming hydromedusae exploit velar kinematics to form an optimal vortex wake, J. Exp. Biol. 209 (11) (2006) 2025–2033.
[28] S.C. Shadden, J.O. Dabiri, J.E. Marsden, Lagrangian analysis of fluid transport in empirical vortex ring flows, Phys. Fluids 18 (2006) 047105.